Neural Comput & Applic (2014) 24:1887–1904
DOI 10.1007/s00521-013-1438-3

ORIGINAL ARTICLE

An ensemble classifier system for early diagnosis of acute lymphoblastic leukemia in blood microscopic images

Subrajeet Mohapatra · Dipti Patra · Sanghamitra Satpathy

Received: 16 January 2013 / Accepted: 22 May 2013 / Published online: 15 June 2013

Abstract Leukemia is a malignant neoplasm of the blood or bone marrow that affects both children and adults and remains a leading cause of death around the world. Acute lymphoblastic leukemia (ALL) is the most common type of leukemia and is more common among children and young adults. ALL diagnosis through microscopic examination of the peripheral blood and bone marrow tissue samples is performed by hematologists and has been an indispensable technique long since. However, such visual examinations of blood samples are often slow and are also limited by subjective interpretations and less accurate diagnosis. The objective of this work is to improve the ALL diagnostic accuracy by analyzing morphological and textural features from the blood image using image processing. This paper aims at proposing a quantitative microscopic approach toward the discrimination of lymphoblasts (malignant) from lymphocytes (normal) in stained blood smear and bone marrow samples and to assist in the development of a computer-aided screening of ALL. Automated recognition of lymphoblasts is accomplished using image segmentation, feature extraction, and classification over light microscopic images of stained blood films. Accurate and authentic diagnosis of ALL is obtained with the use of improved segmentation methodology, prominent features, and an ensemble classifier, facilitating rapid screening of patients. Experimental results are obtained and compared over the available image data set. It is observed that an ensemble of classifiers leads to 99 % accuracy in comparison with other standard classifiers, i.e., naive Bayesian (NB), K-nearest neighbor (KNN), multilayer perceptron (MLP), radial basis functional network (RBFN), and support vector machines (SVM).

Keywords Acute lymphoblastic leukemia · Cell morphology · Quantitative microscopy image analysis · Functional expansion ensemble classifier

1 Introduction

According to the American Cancer Society, cancer or malignant neoplasm is the world's leading cause of death followed by cardiovascular diseases. Cancer can be understood as a group of diseases characterized by: (i) uncontrolled cell division which prohibits programmed cell death and contributes to abnormal growth of tissues, (ii) ability to metastasize (spread), and (iii) eventually compromising the cellular function of the person, which successively may lead to death [1]. Cancer can affect any part of the body, although some cancers are more common or less common than others. According to the Centers for Disease Control and Prevention, 12.7 million people find out each year around the world that they have cancer and 7.6 million people die from cancer. And as per the joint study conducted by Centre for Global Health Research at St. Michael's Hospital, Toronto, and Indian national institutions in India, cancer alone accounted for 8 % of the 2.5 million total male deaths and 12 % of the 1.6 million total female deaths in the year 2010 [2].

S. Mohapatra (✉) · D. Patra
National Institute of Technology, Rourkela 769008, India
e-mail: subrajeets@gmail.com

D. Patra
e-mail: dpatra@nitrkl.ac.in

S. Satpathy
Ispat General Hospital, Rourkela 769005, India
e-mail: sanghamitra.satpathi@gmail.com

Hematological malignancies are heterogeneous group of diseases which includes various forms of leukemia, lymphoma, and myeloma and are characterized by the malignant uncontrolled growth of hematopoietic cells [3]. The development of such malignancies results from an accumulation of genetic mutations in genes involved in regulating cell differentiation and proliferation, leading to aberrant control of these processes. It has been reported that approximately 75,000, 45,000, and 20,500 persons were diagnosed with lymphoma, leukemia, and myeloma, respectively, in 2011 in the USA alone [4]. In India, for the year 2010 approximately the total number of individuals suffering from blood cancer was estimated to be 104,239 [5]. And according to Indian Council of Medical Research (ICMR) by the year 2020, the total number of cancer cases of lymphoid and hematopoietic system is expected to go up to 77,190 for males and 55,384 for females. Even though leukemia starts in the bone marrow and lymphoma in the lymphatic system, both are considered as malignancies of the blood. The duo can affect people of all ages; however, leukemia is more common in children and young adults and people over the age of 60. The majority of leukemia deaths occur in low- and middle-income countries including India, where most of the patients are diagnosed in later stages. In India, leukemia is the most common childhood cancer with relative proportion varying between 25 and 40 % [6] and is the present subject of our study.

Definite genetic processes contribute toward malignant transformation of cells and their progeny forming a clone of leukemic cells [7]. Such neoplastic proliferations of hematopoietic cells are known as leukemia. Based on the severity of the disease, leukemia can be acute or chronic. Acute leukemia can be defined as neoplasms with more than 20 % of blasts in the peripheral blood/bone marrow and is a group of disorders which, if untreated, results in death in few weeks. Acute leukemia comprises a large number of leukemias, and its practical classification is always difficult. However, it can be categorized on the basis of morphologic findings, genetic abnormalities, putative etiology, cell of origin, immunophenotypic qualities, and clinical characteristics. Acute leukemia can be broadly classified into two types:

- Acute myeloblastic leukemia (AML)
- Acute lymphoblastic leukemia (ALL)

Due to advancement in treatment modalities, it is always necessary to subclass the leukemia to assess the prognosis and for the suitable planning of the treatment. The most widely used protocols for leukemia subcategorization are World Health Organization (WHO) classification and French, American, British (FAB) [8]. But, both fundamentally divide leukemias as myeloid and lymphoid types, depending on the origin of the blast cell. Acute lymphoblastic leukemia (ALL) is the single most common pediatric malignancy accounting for one-fourths of all childhood cancers, thus considered as our current research focus. ALL affects both children and adults; however, primarily it is a childhood disease with peak prevalence between the age of 2 and 5 years. According to WHO, ALL subtypes are based on whether the precursor cell is a T or B lymphocyte, whereas FAB classification of ALL is based on morphology and histochemical staining and can be L_1, L_2, or L_3 subtypes.

Currently, microscopic examination of blood samples (peripheral blood/bone marrow) is a standard procedure for a confirmative screening and subtyping of ALL. However, regardless of advanced techniques like flow cytometer, immunophenotyping, and molecular probing, morphological evaluation of stained blood films still remains an economical procedure for the initial screening of ALL [9] across the globe. ALL diagnosis involves distinguishing a healthy lymphocyte from a malignant lymphocyte (lymphoblast) and can be difficult, even for an expert hematologist if the morphological features are not well developed or partially present. Nevertheless, there is always a chance of variability in human-reported diagnosis due to several factors, i.e., improper manual staining, operator fatigue, and inter-observer and intra-observer differences. Analysis of blood samples for hematological inferences is purely qualitative and is based on clinico-pathological experience of the observer. As is the case at most regional cancer centers in India, visual diagnosis is often time-consuming and cumbersome as the number of cases per day is quite high across the country. Manual procedures are often subjected to unacceptable inter- and intra-observer variations [10], resulting in nonuniformity in diagnosis. Due to the prevalence of such uncertainty in manual screening of ALL, the conventional hematological evaluation needs to be strengthened using quantitative microscopy. Such automated procedures aim at avoiding painful biopsies and will facilitate early and precise diagnosis of leukemia. The representative blood microscopic images consisting of a lymphocyte (healthy) and a lymphoblast (malignant lymphocyte) are depicted in Fig. 1.

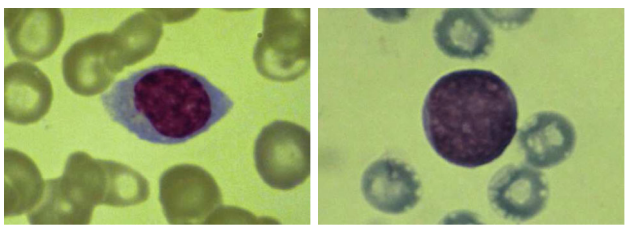

(a) Lymphocyte **(b)** Lymphoblast

Fig. 1 Representative blood microscopic images containing a lymphocyte and lymphoblast

The present study considers the application of machine vision and machine learning techniques for the automated recognition of lymphoblast in Leishman [11]-stained blood microscopic images and facilitates automated ALL screening.

The early detection and complete remission of leukemia are the most challenging tasks of hemato-oncologists. Globally, several research groups are working toward effective treatment of leukemia. According to the literature, very few image-based automated and semiautomated lymphoblast recognition systems have been reported [12–15]. To be particular, a considerable amount of work has been done to achieve the leukocyte or white blood cell (WBC) segmentation [16–19]. Few papers are also devoted toward achieving robust segmentation performance even under variable staining and uneven lighting conditions [20–22]. Moreover, automation of differential blood count or leukocyte classification has been addressed by multiple authors [23–26].

Comaniciu et al. [27] proposed a image-guided decision support (IGDS) system for the automated classification of lymphoproliferative disorders. This system includes an effective cell segmentation module based on mean shift algorithm. While this method demonstrates satisfactory performance for the classification of various malignant lymphomas, the system is yet to be tested for acute leukemia.

Serbouti et al. [28] proposed the use of classification and regression trees (CART) statistical software for the classification of hematological malignancies using the cell markers extracted from images. However, the problems of discrimination of lymphocyte from lymphoblast in blood images have not been addressed exactly. Further, the segmentation scheme used as well as the features involved is not mentioned either.

Foran et al. [12] have reported a method to discriminate among lymphoma and leukemia with a classification accuracy of around 83 %. The method is reported to have successfully worked on 19 lymphoproliferative cases, which is a very small data set to evaluate the performance of the system. Further, the presented method is yet to be validated on ALL cases.

Scotti [29] proposed a method for automated classification of ALL in gray-level peripheral blood smear images. Experiments were conducted on 150 images, and it was concluded that lymphoblast recognition is feasible from blood images using morphological features. However, use of Otsu thresholding in image segmentation and feedforward neural network for feature classification is the cause of low recognition rate.

Markiewicz et al. [30] worked on images of the bone marrow aspirate and proposed a system for automatic recognition of blast cells of myeloid series. While this method is able to recognize myeloblast up to certain extent, the system is yet to be tested with sample blast cells of lymphoid series (lymphoblasts).

Halim et al. [31] reported an automated blast counting method for acute leukemia detection in blood microscopic images. Histogram-based thresholding is performed on *S*–component of the *HSV* color space, followed by morphological erosion for image segmentation. Determination of accurate threshold to separate nucleus from cytoplasm is important, and no specific methods have been presented for its estimation. Further, the features used as well as classifier employed for disease recognition have not been mentioned.

Various commercial hematology software having a provision for leukocyte image analysis is also available over the last few years. Among them, CellarVision Diffmaster Octavia [32] and Cellarvision DM96 [33] have been a trusted brand and recognize WBC by scanning the entire blood slide at a lower magnification and using specific features of WBC. Preclassification is performed without leukocyte segmentation on the cropped subimage. Thus, the reliability of the current system is less as accurate leukocyte classification requires proper cytoplasm and nucleus segmentation [19]. The absence of image segmentation module prohibits accurate differentiation of lymphocyte and lymphoblast, hence no automated ALL recognition.

Both acute lymphoblastic leukemia (ALL) and acute myeloblastic leukemia (AML) differ much in terms of nucleus chromatin and cell morphology. Image-based differentiation of benign and malignant cell samples is mostly based on cell morphology, texture, and color due to histochemical stain. Even though the aforementioned schemes work well for automated myeloblast recognition, they may not be applicable to lymphoblasts also. Moreover, due to considerable difference between ALL and AML, independent schemes are required to be developed for the recognition of each type of blast, i.e., myeloblast and lymphoblast.

Thus, the main contribution of this study is the development of independent segmentation and recognition techniques for the automatic identification of lymphoblast in blood microscopic images. Figure 2 shows the proposed computational approach toward acute leukemia detection. The outline of this paper is as follows. Section 2 describes the process of microscopic image acquisition and the algorithm for cropping subimages. Shadow C-means clustering-based lymphocyte image segmentation is outlined in Sect. 2.5. Section 3 presents a detailed analysis of the applied feature extraction techniques. The process of feature value normalization and the procedure for the selection of statistically significant features are discussed in Sect. 4. A brief overview of various standard classifiers is

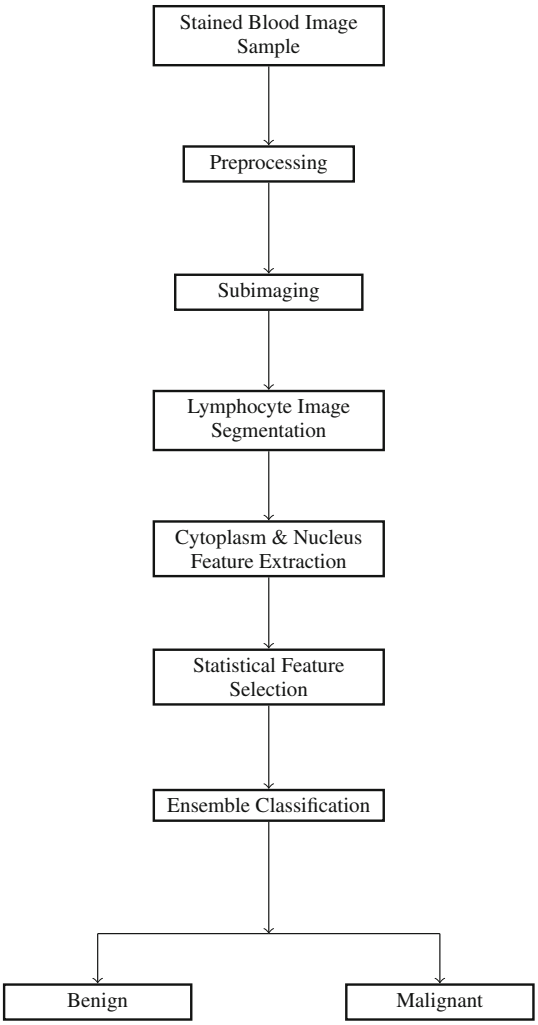

Fig. 2 Block diagram of the proposed automated ALL diagnosis system

demonstrated in Sect. 5. In Sect. 6, use of ensemble of classifiers for automated ALL recognition is introduced. Experimental results and discussion are reported in Sect. 9. Finally, conclusions are summarized in Sect. 10.

2 Materials and methods

In this section we describe the details of the images used for the work and layout of the proposed system, as presented in the following subsection.

2.1 Study subject selection and sample preparation

Patients were enrolled for this study according to stringent inclusion and exclusion criteria. Participants for this study, which include children, adolescents, and adults, were clinically diagnosed with ALL at the Department of Hematology, Ispat General Hospital, Rourkela, India. With proper informed consent, a total of 54 patients with ALL were considered for the study. All these patients were clinically examined and were advised to undergo peripheral blood and/or bone marrow examination. Subsequently, blood or tissue (bone marrow) samples were collected from the patients. A total of 50 normal samples for the study were also obtained from patients undergoing routine differential blood count. Samples of those patients who did not have clinical history of leukemia or any serious disorders were only considered, which may manipulate the blood cell morphology. Peripheral blood smear and bone marrow tissue sections were prepared and then stained with Leishman stain [11] for microscopic visualization. Among all collected blood samples, a joint panel of hematologists confirmed 54 specimens with ALL and 50 specimens were certified as healthy samples without any characteristics of ALL.

2.2 Hematological image acquisition

Blood microscopic images of Leishman [11]-stained peripheral blood or bone marrow samples were optically grabbed by Zeiss Observer microscope (Carl Zeiss, Germany) under 100X oil-immersed setting and with an effective magnification of 1,000 at Ispat General Hospital, Rourkela, India. Each grabbed digital image is represented using three fundamental colors (red, green, and blue) and is stored in an array of size 1,024 $\times$ 1,024.

2.3 Preprocessing

The presence of noise and acquisition of blood microscopic images under uneven lighting conditions necessitates preprocessing. This is achieved using selective filtering [34] and contrast enhancement.

2.4 Subimaging

Peripheral blood smear images are relatively larger with more than one leukocyte per image. However, the desired region of interest (ROI) must contain a single lymphocyte only for the detection of ALL. This is desired since each lymphocyte in the entire blood smear image has to be evaluated for differentiating an immature lymphocyte (lymphoblast) from a mature one. Therefore, K-means [35] clustering was performed using RGB color features on the entire blood smear image to obtain the nucleus image as one of the cluster outputs [36]. When run repeatedly, K-means clustering often results with different cluster outputs due to random initialization of center. Thus, average intensity value of individual color (RGB) planes for each clustered image is used to recognize the cluster

representing the nucleus image. This identified clustered output represents nucleus image and contains nucleus of all the leukocytes present in the entire blood smear. To crop a subimage around each nucleus, a bounding box is required to be drawn around a center point. The coordinates of the center point can be determined by averaging the coordinates of each pixel in the object [37]. This center point is known as center of mass and is obtained for each nucleus using the binary version of the nucleus image. Once the coordinates of the center of mass are obtained for each nucleus, a rectangular subimage is cropped from the original image. This entire process results in subimages containing a single leukocyte only with an assumption that there are no touching cells. The subimaging steps are illustrated in Fig. 4. Sample subimages containing a single lymphocyte are shown in Fig. 5. It should be observed that along with the red blood cells (RBC) each image can contain a combination of neutrophils, eosinophils, basophils, lymphocytes, or monocytes. The problem of leukocyte classification or automated differential blood count has been investigated by several researchers. Implementation of such schemes will serve as lymphocyte identifier module in our proposed system and will facilitate the complete automation of the ALL disease recognition system. However, as ALL is a disease of lymphocytes, we are interested in images that contain lymphocytes only. Therefore, in the present study each blood smear image in the available data set is assumed to contain a particular type of leukocyte, i.e., lymphocyte only along with RBC. Two-sample, Leishman-stained peripheral blood smear image containing a single lymphocyte is depicted in Fig. 3.

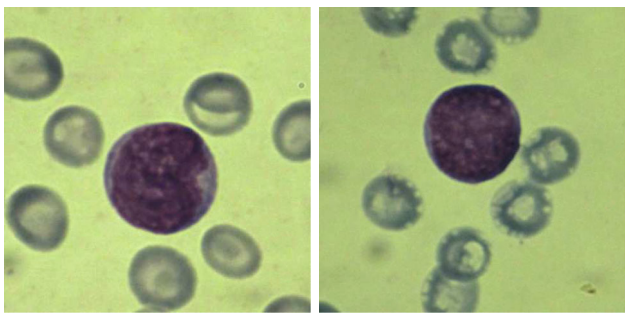

(a) IGH465 **(b)** IGH469

Fig. 3 Representative microscopic image of peripheral blood smear under 100*X* magnification

2.5 Lymphocyte image segmentation using shadowed C-means (SCM) clustering

Image segmentation of blood images is the foundation for all automated image-based hematological disease recognition systems including ALL. Therefore, in this study, a novel Shadowed C-means (SCM) clustering–based approach toward lymphocyte image segmentation is performed in $L^*a^*b^*$ (*CIELAB*) color space. This color space

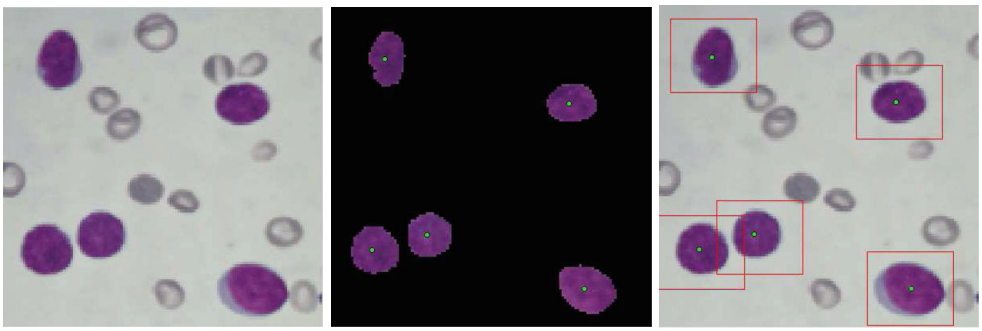

(a) Original (IGH1) **(b)** Detected nucleus **(c)** Detected sub–images

Fig. 4 Subimage detection using K-means clustering and bounding box

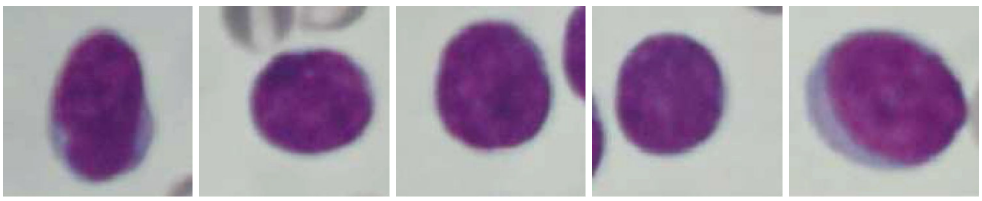

(a) IGH1a **(b)** IGH1b **(c)** IGH1c **(d)** IGH1d **(e)** IGH1e

Fig. 5 Cropped subimages (lymphocytes)

consists of a luminosity layer L and a set of chromaticity layers a and b. The color information is present in the a and b layers only. Transforming the blood microscopic images from RGB to *CIELAB* reduces the color dimension from three (RGB) to two (a and b) and facilitates faster color-based image segmentation. SCM clustering is used to classify each pixel into one of the three regions, i.e., cytoplasm, nucleus, and background. The proposed segmentation approach is applied on each subimage to extract the nucleus and cytoplasm from the background. SCM clustering algorithm for lymphocyte image segmentation is discussed here:

1. Let I_{rgb} represent an original lymphocyte image in RGB color space.
2. Apply $L^*a^*b^*$ color space conversion on I_{rgb} to obtain the $L^*a^*b^*$ image, i.e., I_{lab}.
3. Construct the input feature vector using a^* and b^* components of I_{lab}.
4. Each data pattern of the feature vector is assigned to an appropriate class using Shadowed C-means algorithm.
5. Obtain the labeled image from the classified feature vector.
6. Reconstruct the segmented RGB color image for each class.

To visualize the subjective performance, segmented outputs for mature lymphocytes (healthy) as well as for immature lymphocytes (lymphoblast) using the proposed SCM clustering approach are presented in Figs. 6 and 7, respectively. A more detailed explanation of the proposed SCM-based lymphocyte image segmentation can be found in our previous work [38].

Discriminative features are extracted from each segmented morphological region (cytoplasm and nucleus) and are fed to an ensemble of classifiers, to aid in the automatic diagnosis of ALL by differentiating lymphoblast from lymphocytes.

3 Feature extraction

The criteria during diagnosis or in the follow-up of ALL are based on the percentage of lymphoblast present in the peripheral blood or bone marrow samples. The presence of more than 20 % of lymphoblasts in peripheral blood or

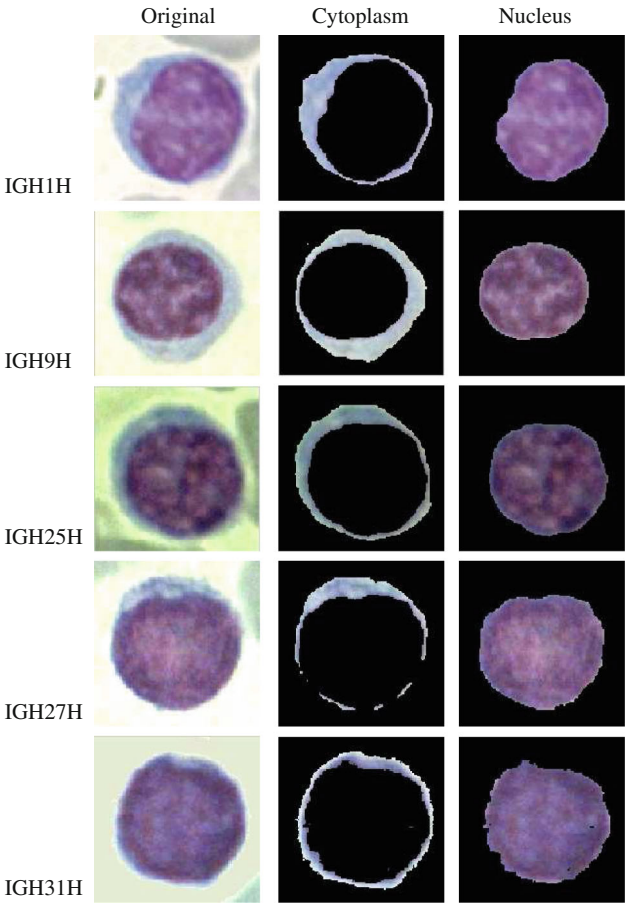

Fig. 6 Segmentation results for healthy mature lymphocytes using SCM clustering approach

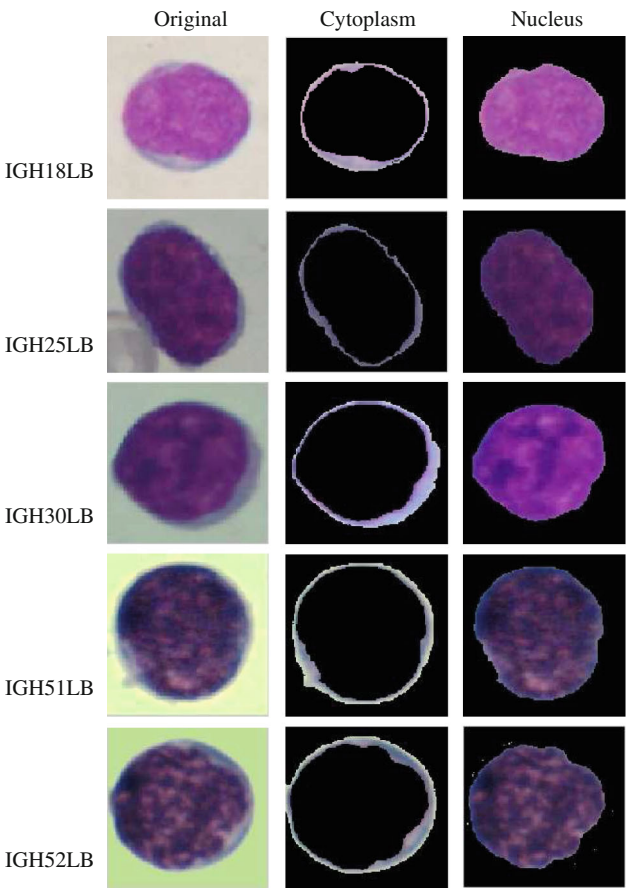

Fig. 7 Segmentation results for immature lymphocytes (lymphoblasts) using SCM clustering approach

bone marrow samples is labeled as ALL [7]. Morphologically, lymphoblast is characterized by large nucleus, having an irregular size and shape, the nucleoli are prominent, and the cytoplasm is scarce and intensely colored. Nucleus and cytoplasm of lymphoblast reflect morphological and functional changes in comparison with lymphocytes and play a main role in the assessment of malignancy in blood samples. The current visual criteria for the recognition of lymphoblasts in blood samples are summarized in Table 1 and are followed by most of the hematologists across the globe [39]. Analysis of the above table reveals marked differences in morphology among mature lymphocyte (small and large) and lymphoblast and is the basis of ALL diagnosis. As per expert's observation, it was noticed that in few samples the cell size of large lymphocytes equates to that of microblasts. In such samples, other morphological parameters, i.e., *N*/*C* ratio and nucleus chromatin distribution, are considered as essential discriminating factors for the diagnosis process. Further, it should also be remembered that the above features may not be distinct for the recognition of blasts individually. Accordingly, an amalgamation of all the features is adapted by expert hematologists for the final assessment of a *PBS* sample. Despite all, human evaluation of *PBS* is always subjective and time-consuming in nature. Therefore, to facilitate hematologists with a reliable tool for the diagnosis and follow-up of ALL, a set of novel quantitative features are presented here using an image processing approach.

The basis for the differentiation of lymphocyte from lymphoblast as per experienced hematologists can be grouped as the following two types of characteristics, i.e., nuclear changes (variation in shape and size, chromatin pattern) and cytoplasmic changes (amount of cytoplasm and protein accumulation). In this work, we suggest some quantitative features for nucleus and cytoplasm region of a lymphocyte, which is correlated directly with the actual cytological features and aids in the computer processing of lymphocyte images. Among them, few features are directly measurable, while others can be computed from the measured data and each of them belongs to one of the three broad categories, i.e., morphological, textural, and color features. A brief description of the proposed computed cell features is summarized in Table 2 and is used to develop an automated ALL recognition system. Further, a detailed description about the clinical importance of each computed feature is presented below.

The following morphological, textural, and color features are measured from the binary, gray, and color image version of the nucleus and cytoplasm image, respectively, of the individual image regions of each lymphocyte image.

1. Area (F1–F2): Individual area is computed by counting the total number of pixels present in the binary version of the nucleus and cytoplasm image, respectively.
2. Nucleus/cytoplasm ratio (F3): It is a measurement to indicate the maturity of a cell and is the ratio of the size of the nucleus to the size of the cytoplasm of that lymphocyte.
3. Cell size (F4): Entire cell area is computed by adding individual cytoplasm and nucleus area.
4. Perimeter (F5): The perimeter of the nucleus is obtained by counting the total number of pixels representing the nucleus boundary.
5. Form factor (F6): It is a shape parameter derived from the basic cellular measurements, i.e., area and perimeter. It can be mathematically defined as

$$Formfactor = \frac{4 \times \pi \times Area}{\text{Perimeter}^2} \quad (1)$$

6. Roundness (F7): It is the degree to which the nucleus shape differs from that of a circle and can be defined as

Table 1 Morphological characteristics—lymphocyte and lymphoblast

Feature	Lymphocyte		Lymphoblast
	Small	Large	
Cell size	Small	Large	Large
N/C ratio	Low	Low	High
Nucleus shape	Round or oval	Round or oval	Indented
Nucleus size	Less	Less	Large
Nuclear chromatin	Closed	Closed	Open
Nucleoli	Usually absent	Usually absent	Distinct
Nucleus boundary	Smooth	Smooth	Rough
Amount of cytoplasm	Scanty	Abundant	Scanty
Nucleus color	Blue–purple	Blue–purple	Sparse Red–purple
Cytoplasmic color	Light clear sky blue	Light clear sky blue	Deep blue
Cytoplasmic boundary	Rough	Rough	Smooth

Table 2 Computed cell features of lymphocytes extracted using image processing

Features		Description
Cytologic	Computed	
Nucleus size	Nucleus area	Number of pixels in the nucleus region
Cytoplasm size	Cytoplasm area	Number of pixels in the cytoplasm region
Lymphocyte size	Lymphocyte area	Sum of all the pixels in the cytoplasm and nucleus region
Nucleus contour	Nucleus perimeter	Number of pixels in the contour of the nucleus
Nucleus shape	Nucleus shape	Nucleus region shape in terms of form factor, roundness, compactness, and elongation
Nucleus boundary roughness 1	Fractal dimension	Hausdroff dimension (HD) value of the nucleus contour
Nucleus boundary roughness 2	Contour signature	Variance, skewness, and kurtosis of all the distances between nucleus centroid and contour pixels
Texture 1	Wavelet coefficients	Mean and variance of approximation, horizontal and vertical matrix components of nucleus and cytoplasm region
Texture 2	GLCM	Contrast, correlation, energy, homogeneity, and entropy statistics are derived from the GLCM matrix of the nucleus and cytoplasm region
Texture 3	Fourier transform	Mean, variance, skewness, and kurtosis of the frequency components of the nucleus region
Color	Region color	Individual nucleus and cytoplasm region color in terms of mean intensity of individual red, green, blue, hue, saturation, and lightness component

$$Roundness = \frac{4 \times Area}{\pi \times \text{Maximum Diameter}^2} \quad (2)$$

7. Length/diameter ratio (F8): Length-to-diameter (L/D) ratio is the ratio of the major axis length and minor axis length of the nucleus region.
8. Compactness (F9): It is a numerical measure representing the degree to which a shape is compact and is mathematically represented as

$$Compactness = \frac{\sqrt{\frac{4}{\pi} \times Area}}{\text{Maximum Diameter}} \quad (3)$$

9. Nucleus boundary roughness: Nuclear boundary irregularity is an important diagnostic feature of ALL. To measure such deformation accurately in quantitative manner, fractal geometry and contour signature can be used and a detailed explanation is presented below.

   (a) Fractal geometry (F10): It is used to measure the irregularities of the nucleus margin of lymphocytes and aids in the differentiation of malignant lymphocytes (lymphoblast) from benign ones. Irregularity and complexity are the main properties of organized biological matter including human tissue, cells, and subcellular components. However, traditional Euclidian geometry is incapable of objective assessment of human cellular components including measurement of nucleus boundary irregularity of lymphocytes. Unlike Euclidian geometry, fractal geometry represents objects in noninteger dimension and is an invincible tool for representing irregular-shaped objects including erratic ramified lesions of tumors and irregular shape of malignant cells [40].

   Due to strong theoretical reasons and as per published studies, there is a strong evidence of using fractal geometry in the quantitative assessment of cellular pathology. However, the use of fractals in hematopathology is limited, and in this paper we present the use of fractals as a measure of nuclear margin irregularity. Even though many fractal properties have been defined, Hausdroff dimension (HD) is one of the most important since it provides an accurate objective measure of irregularity or coarseness. Several approaches for the estimation of HD or D_f (F10) are available in the literature; however, the most common among them used in biological sciences may be summarized as follows:

   - Modified pixel dilation
   - Perimeter–area
   - Ruler counting
   - Box counting

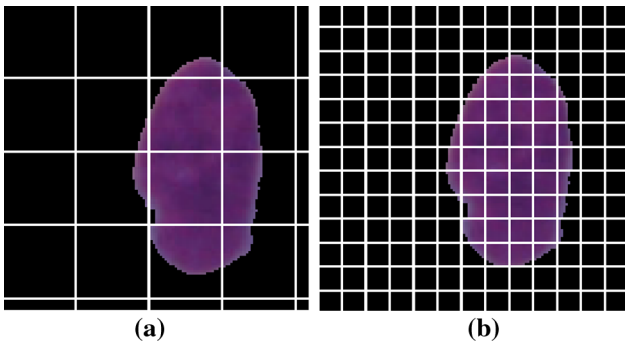

Fig. 8 Boxes of different pixel lengths superimposed over the segmented nucleus image

Out of these, the box counting method is more popular due to its easier implementation and is based on self-similarity. In this method, we cover boxes of different pixel lengths over the digitized version of the segmented nucleus image (Fig. 8). The Hausdroff dimension D_f of a bounded set A in Euclidean n-space can be derived from the relation:

$$D_f = \lim_{r \to 0} \frac{\log(N_r)}{\log(\frac{1}{r})} \tag{4}$$

where N_r is the least number of distinct copies of A in the scale r.

(b) Contour signature: The shape of the lymphocyte nucleus is well known in benign cases and does not deviate much from an average shape. However, genomic alterations in malignant cells affect the structure of the nucleus and cause deviation from the average shape. Contour signature is an additional measure to supplement fractal dimension in characterizing nucleus boundary and has been presented here. In this method the dimensionality of the representation of the contour is reduced from two to one by converting from a coordinate-based representation to distances from each contour point to a reference point. A suitable reference point is centroid or center of mass of the contour, whose coordinates can be defined as:

$$\begin{aligned} \bar{x} &= \frac{1}{M} \sum_{n=0}^{M-1} x(\mathrm{n}) \\ \bar{y} &= \frac{1}{M} \sum_{n=0}^{M-1} y(\mathrm{n}) \end{aligned} \tag{5}$$

where (x, y) are the coordinates of the pixels along the contour and M is the total number of pixels on the nucleus contour. Nucleus contour of a benign (healthy) and a malignant (lymphoblast) lymphocyte sample is depicted in Fig. 9. The diamond symbol represents the centroid of the nucleus contour, and $d(n)$ is the Euclidian distance between the centroid and each nucleus contour point.

The signature of a contour provides general information on the nature of the contour such as its smoothness or roughness. It is evident that the smooth nucleus contours of benign or healthy lymphocyte possess a smooth signature, whereas the malignant lymphocyte (lymphoblast) nucleus has a rough signature with several significant rapid variations over its period. The signature can be defined by the variance (F11), skewness (F12), and kurtosis (F13) of all the distances between centroid and nucleus contour points that will be significantly different in benign and malignant samples.

Based on past experience of hematologist, malignant lymphocytes are characterized by smooth cytoplasmic boundary and can be an essential feature for lymphoblast recognition. Therefore, HD (F14) and contour signature (F15–F17) features were also measured for the cytoplasm region of each lymphocyte image sample.

10. Texture: Changes in the chromatin distribution reflects the organization of DNA in lymphocyte nucleus and is an essential diagnostic descriptor for classifying malignant lymphocytes (lymphoblast) from benign ones. Leishman staining of blood samples enables the visualization of chromatin distribution of lymphocyte nucleus in the form of texture. Genetic modifications are responsible for textural changes and are visible during the transition from normal to malignant. Such textural transformation can be quantified using Haar wavelet–based and Haralick's feature–based methods and is presented below.

(a) Wavelet texture features (F18–F23): Haar wavelet texture features are computed by applying a combination of high pass and low pass to each lymphocyte nucleus image [41]. A_n is the approximation image and is obtained by low-pass filtering of the nucleus image, whereas the H_n, V_n, and D_n are the detailed coefficients and are obtained through high-pass filtering in horizontal, vertical, and diagonal direction.

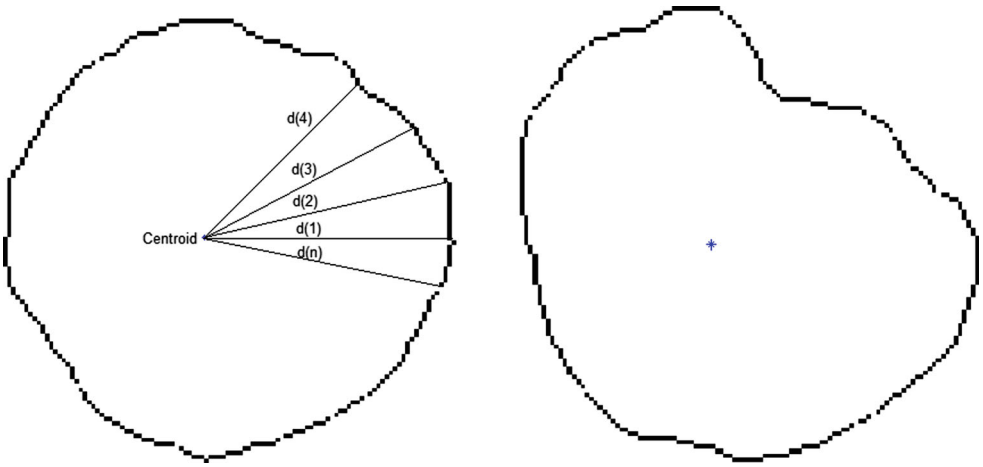

Fig. 9 Nucleus contour of lymphocyte samples

(a) Benign **(b)** Malignant

A texture feature vector for each gray-scale version of lymphocyte nucleus image consists of wavelet coefficients obtained by taking mean and variance of A_n, H_n, and V_n components. Due to the absence of classification information in diagonal coefficients, D_n component is excluded from feature extraction [42].

(b) Haralick's texture features: The gray-level co-occurrence matrix (GLCM) method is a way of extracting Haralick's texture features. A co-occurrence matrix is a two-dimensional matrix, in which both the rows and the columns represent a set of possible image values. GLCM can be defined as $G_d[i, j] = n_{i,j}$, where n_{ij} is the number of occurrences of the pixel (i, j) lying at distance d in the image. The co-occurrence matrix G_d has a dimension $n \times n$, where n is the number of gray levels in the image. Statistical measures, i.e., contrast (F24), correlation (F25), homogeneity (F26), energy (F27), and entropy (F28), are computed from the co-occurrence matrices using offsets such as (1, 0), (−1, 0), (0, 1), and (0, −1) [43] and are used to differentiate benign and malignant nucleus of lymphocyte image data samples.

(c) Fourier descriptors (F29–F32): This transform is useful in highlighting the dominant orientations of the DNA structures present in the lymphocyte nucleus region. Feature descriptors used here for texture quantification are based on two-dimensional discrete Fourier transform (DFT). Statistics, i.e., mean, standard deviation, skewness, and kurtosis, are computed over the nucleus image in the frequency domain obtained using discrete Fourier transform.

11. Color: Excessive pigmentation in lymphocyte nucleus results in hyperchromatism and is an important characteristic appearing in malignant lymphocytes. Chromatin abnormality results in increased staining capacity of nuclei. Such modification in DNA content of nuclei is visible in the form of change in color intensity in ALL. This color change during transition from normal to malignant is measured as mean color intensity in RGB and HSV color space, and a set of six features, i.e., μ_R (F33), μ_G (F34), μ_B (F35), μ_H (F36), μ_S (F37), and μ_V (F38), are computed to represent the change in color, where μ represents the mean intensity for the red (R), green (G), blue (B), hue (H), saturation (S), and value (V) components, respectively. Similar measurement of color features (F39–F44) was also performed for the cytoplasm region and is considered as a member of the feature vector for ALL recognition. It is observed that color features have low computational cost in comparison with texture features.

Combination of all three types of features generates a total of 44 features of which 17, 15, and 12 are shape or size, texture, and color features, respectively.

4 Data normalization and feature selection

Prior to classification, it is necessary to normalize the data set with dissimilar range of values and to estimate the discriminating capability of each feature or a set of features among the labeled classes.

Combination of variables with nonuniform magnitudes results in masking of lower-magnitude data by higher-magnitude data due to the fact that sheer magnitude of the inputs generates larger weights associated with them. Therefore, normalization is an essential procedure to transform the input features into a similar range so that true influence of variables can be ascertained [44]. Feature

normalization is also beneficial in making the neural network training process smoother. A popular approach is to standardize the data set with respect to the mean and standard deviation using a linear transformation. The above linear transformations are performed for each individual variable. To achieve data normalization, each input variable or feature is treated individually, and for each feature x_i in the training set, the mean $\bar{x}_i$ and variance σ_i^2 are calculated. Using this each input variable or feature can be normalized as

$$x^n{}_{T_i} == \frac{x^n{}_i - \bar{x}_i}{\sigma_i} \tag{6}$$

where $x^n_{T_i}$ is the normalized (transformed) value of the nth observation of the variable x_i. Such an operation results in a new set of normalized features with zero mean and unit standard deviation.

Selection of an appropriate set of features is important and strongly affects classifier performance. Filter and wrapper methods are the widely used feature selection methods. Feature selection using filter method is a process of obtaining features with strong discrimination power and is used in this paper. Independent-sample "t" test is one such popular approach to determine the statistical significance of the extracted features [43, 45]. Out of all the 44 extracted features, 32 features were found to be statistically significant (p value < 0.05) using t test and participate in the classification process.

5 Classification

In pattern recognition, classifiers are used to divide the feature space into different classes based on feature similarity. Depending on the number of classes, each feature vector is assigned a class label which is a predefined integer value and is based on the classifier output. Each classifier has to be configured such that the application of a set of inputs produces a desired set of outputs. The entire measured data are divided into training and testing data sets. The training data are used for updating the weights, and the process of training the network is called learning paradigms. The remaining test data were used for validating the classifier performance. In this study, we propose the use of an ensemble of classifiers for labeling each lymphocyte subimage as healthy or malignant sample based upon a set of measured features. Performance of the extracted features in classification was also tested with five other standard classifiers, i.e., naive Bayesian, KNN, MLP, RBFN, and SVM. Suitable parameter tuning was performed for each classifier to achieve optimum accuracy, and the same training and testing data sets were used for all while evaluating their individual classifier performances.

5.1 Naive Bayesian

Bayesian classification is based on Bayes' theorem and is an important supervised statistical classification method used in pattern recognition. The working of such a classifier is based on Bayes' decision theory, and the principle of decision is to choose the most probable one [43, 46]. It is designed specifically for classification task with features that are independent of one another within each class. However, with the naive Bayes classifier, although the independence assumption may not be valid, the final performance may still be good.

5.2 K-nearest neighbor

K-nearest neighbor (KNN), even though a simple classifier, yet yields good classification accuracy. Using KNN classifier, each unknown test sample is assigned to a class to which majority of its K-nearest neighbors belong [47].

5.3 Multilayer perceptron

Multilayer perceptron (MLP) is the most popular supervised neural classifier for which many learning paradigms have been developed and are capable of performing nonlinear mapping. In MLP networks there exists a nonlinear activation function. The hidden layers along with the connected synaptic weights make the MLP network capable for such nonlinear mappings [34]. Backpropagation is a general supervised method for iteratively calculating the weights and biases of the MLP network.

5.4 Radial basis functional neural network

Radial basis functional network (RBFN) has gained considerable attention as an alternate to multilayer perceptron (MLP) trained by the backpropagation algorithm [48]. The basis functions are embedded in a two-layer neural network, where each hidden unit implements a radial activated function. There are no weights connected between the input layer and hidden layer. Finding the appropriate RBF weights is called network training, and least mean square (LMS) learning algorithm is mostly used.

5.5 Support vector machines

Support vector machines (SVM) were introduced by Vapnik [39] and have the capability to distinguish two classes. SVM first use a nonlinear mapping function for transforming the input data from the observation space to a higher-dimensional feature space and then create a maximum margin hyperplane to separate the two given classes [49]. Nonlinear mapping functions transform the nonlinear

separation problem in the input plane into a linear separation problem in feature space facilitating easier classification in the higher-dimensional feature space.

5.6 Ensemble of classifiers

Ensemble-based systems or multiple-classifier systems have been popular and drawing a very significant attention of the researchers over the last few decades [50–52]. Multiple-classifier systems are more preferable than their single-classifier counterparts due to several reasons, and a few important reasons among them are presented in Table 3.

There are many other scenarios where ensemble of classifiers have shown to produce favorable results, and the implementation details can be found in Kuncheva's work [53].

Classifier diversity is a desirable property of all multiple-classifier systems and is achieved through several possible ways. Some of the possible ways to achieve diversity is by using different data sets, training parameters for the training of each individual member, and by the combination of entirely different sets of classifiers. It is always needed to have a set of classifiers with adequately different decision boundaries and to build an ensemble that is as diverse as possible. A suitable strategy is always needed to be framed for combining the outputs of individual classifiers and to build an ensemble in such a way that the potential of correct decisions is amplified and incorrect ones are ruled out [51].

Another key issue in combining classifiers is to frame suitable combination rules. One such approach is combination rules that apply to class labels only and is based on classification decision output. Multiple-classifier systems combine class labels obtained from the individual ensemble members to predict the final class label. Specific predefined rules have been framed and are used for the selection of final class label from the individual class labels. Popular among them are majority voting, weighted majority voting, behavior knowledge space, and Borda count. The most powerful rule appears to be majority voting rule and is used in this paper.

Table 3 Reasons for using ensemble of classifiers

Reason	Description
Statistical	Reduces the chance of poor selection
Large data set	Feasibility of training is less
Limited data set	Resampling techniques are very effective
Divide and conquer	Complex decision boundary to be learned
Data fusion	Useful with heterogeneous features

In general, enhanced ALL recognition performance is observed through the deployment of an ensemble of classifiers and a detailed description of which is presented in the following section.

6 Ensemble of classifiers for automated ALL recognition

It is highly desirable to maintain a very high recognition and a low error rate in all automated disease recognition systems. However, it is difficult for a single classifier to achieve this for a complex pattern recognition problem, i.e., lymphoblast count in blood images. In an effort to deal with such challenges, an ensemble of classifiers–based approach for the classification of extracted lymphocyte features is investigated here. An ensemble-based system, also known as multiple-classifier system (MCS), predicts by combining several diverse classifiers. Diversity may be achieved by using entirely different set of classifiers and also by using a different training data set for each classifier [54]. The idea is that each ensemble member will generate a different decision boundary and make a different error, and suitable combination of classifiers will reduce the total error. In order to promote diversity, bagging [55] is used to train each ensemble member using a randomly drawn subset of the training data. Class labels generated by individual classifiers are combined using majority voting, and the class label chosen by most classifiers is the final ensemble decision. The block diagram of a standard ensemble of classifiers (EOC) for feature classification is shown in Fig. 10.

In general, there are two alternatives to build an ensemble of classifiers. Either we have a single base classifier with variable architectures and parameter settings as ensemble members, or we have a collection of different independent classifiers as members of the ensemble. In the first phase of our implementation, MLP was considered as the base classifier, and variable architectures of MLP obtained using different parameter settings were considered to build the ensemble. However, during the second phase, a combination of classifiers with different topologies were considered for building the ensemble. In general, the ensemble of three individual classifiers, i.e., K-nearest neighbors (KNN), multilayer perceptron (MLP), and support vector machines (SVM), were found to perform best with the available data and were considered for final lymphoblast recognition. Therefore, only the experimental results of the second phase of implementation of ensemble of classifiers with different topologies are presented in Sect. 9.

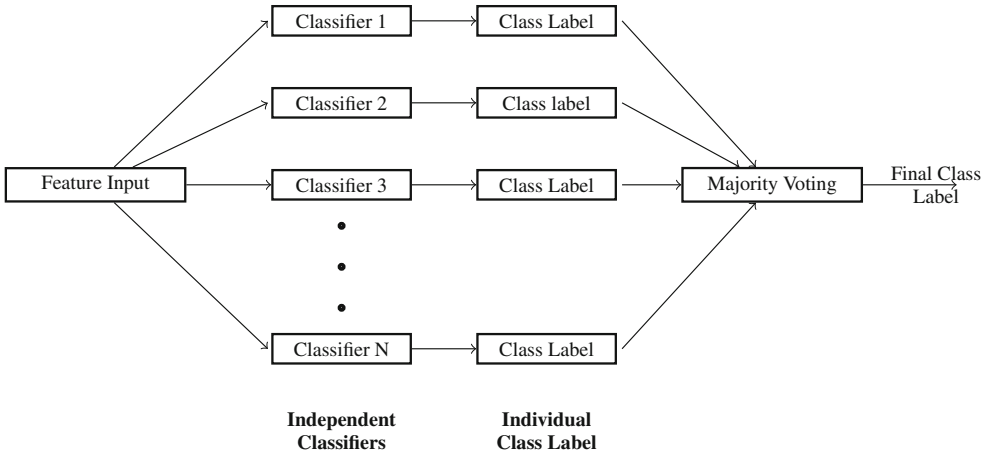

Fig. 10 An ensemble of classifiers for feature classification

7 Validation

In view of the fact that the data set used in this study is small, *k*-fold cross-validation [56] resampling technique is employed for the training and testing of the classifiers for the extracted lymphocyte features. Considering the value of *k* as 5, the whole data set is randomly divided into five parts, in which each class is represented in approximately the same proportions as in the original data set. Three parts of the data are used for classifier training (training set), and the rest two parts are considered for evaluation (testing set). Thus, the procedure is executed a total of five times with different combination of training and testing data. Finally, the five performance estimates are averaged to yield an overall estimate of the classifier performance in terms of accuracy, specificity, and sensitivity.

8 Performance analysis

Performance evaluation is mandatory in all automated disease recognition systems and is conducted in this study to evaluate the ability of the above classifiers for the screening of leukemia in *PBS* images. In practice, performance metrics, i.e., accuracy, specificity, and sensitivity, are calculated from a confusion matrix (Table 4) which represents the differences in opinion between the hematologist and the classifier.

Table 4 Confusion matrix for classifier performance evaluation

Classifier output	Hematologist opinion	
	Positive (Leukemia)	Negative (Healthy)
Positive (Leukemia)	TP	FP
Negative (Healthy)	FN	TN

In a binary classification problem, positive is considered as identified and negative as rejected. So in general, *TP*, *TN*, *FP*, and *FN* can be defined as:

TP (true positive): Correctly identified
TN (true negative): Incorrectly identified
FP (false positive): Correctly rejected
FN (false negative): Incorrectly rejected

In this study, performance measure, i.e., accuracy, specificity, and sensitivity, is calculated to assess the diagnostic accuracy of the above classifiers and can be formulated in terms of *TP*, *TN*, *FP*, and *FN*. The performance measures can be written as:

$$Accuracy = \frac{TP + TN}{TP + FP + TN + FN} \times 100\%$$

$$Sensitivity = \frac{TP}{TP + FN} \times 100\%$$

$$Specificity = \frac{TN}{TN + FP} \times 100\%$$

As the validation procedure employed is fivefold cross-validation, the learning procedure is executed a total of 5 times on different training sets and accuracy, specificity, and sensitivity are recorded each time. Finally, the average of all the five readings yields the overall estimate of each measure.

9 Results and discussion

The proposed scheme was implemented using Matlab 7.8, and experimental simulation was performed using an Intel Core i5 3.20 GHz PC, along with 2 GB RAM running on Windows 7 professional operating system. An automated system for the diagnosis of leukemia in blood microscopic images has been developed, and experiments were

Table 5 Morphological features extracted from nucleus and cytoplasm of normal and malignant lymphocytes

Feature index	F–eatures	Malignant $\mu \pm \sigma$	Normal $\mu \pm \sigma$
1	Nucleus area*	8.30e+03 ± 1.03e+03	7.31e+03 ± 1.27e+03
2	Cytoplasm area*	1.43e+03 ± 5.3721e+05	2.465e+03 ± 0.71e+03
3	Nucleus/cytoplasm ratio*	6.16 ± 2.93	3.34 ± 1.57
4	Cell size*	9.08e+03 ± 1.60e+03	8.44e+03 ± 0.43e+03
5	Nucleus perimeter*	308.29 ± 703.74	300.60 ± 602.65
6	Nucleus form factor*	0.81 ± 0.06	0.86 ± 0.04
7	Nucleus roundedness*	0.85 ± 0.07	0.87 ± 0.04
8	LD ratio	1.16 ± 0.10	1.16 ± 0.14
9	Nucleus compactness	0.92 ± 0.04	0.93 ± 0.05
10	HD (Nucleus)*	1.21 ± 0.03	1.19 ± 0.02
11	Nucleus CI (variance)*	1.59e-2 ± 1.55e-2	1.50e-2 ± 1.66e-2
12	Nucleus CI (skewness)*	0.45 ± 0.37	0.39 ± 0.24
13	Nucleus CI (kurtosis)*	2.41 ± 0.83	2.27 ± 0.54
14	HD (cytoplasm)*	1.20 ± 0.03	1.21 ± 0.03
15	Cytoplasm CI (variance)*	1.35e-2 ± 1.83e-2	0.67e-2 ± 1.21e-2
16	Cytoplasm CI (skewness)*	0.35 ± 0.33	0.41 ± 0.44
17	Cytoplasm CI (kurtosis)*	2.31 ± 1.31	2.64 ± 1.94

* Significant based on *t* test

Table 6 Texture and color features extracted from nucleus of normal and malignant lymphocytes

Feature index	Features	Malignant $\mu \pm \sigma$	Normal $\mu \pm \sigma$
18	Fourier coefficient (mean)*	2.79e+07 ± 1.19e+07	6.41e+07 ± 4.85e+07
19	Fourier coefficient (variance)*	2.16e+39 ± 4.2040e+39	45.75e+39 ± 46.95e+39
20	Fourier coefficient (skewness)	2.53 ± 0.41	2.67 ± 0.33
21	Fourier coefficient (kurtosis)	20.89 ± 4.57	21.85 ± 18.79
22	Avg. of Haar A coefficient*	152.99 ± 63.11	173.11 ± 34.95
23	Avg. of Haar H coefficient	7.38 ± 1.95	7.58 ± 1.59
24	Avg. of Haar V coefficient*	7.51 ± 2.08	7.89 ± 1.49
25	Variance of Haar A coefficient*	1.46e+03 ± 1.07e+03	1.34e+03 ± 0.50e+03
26	Variance of Haar H coefficient	0.23e+03 ± 0.16e+03	0.23e+03 ± 0.09e+03
27	Variance of Haar V coefficient*	0.25e+03 ± 0.18e+03	0.24e+03 ± 0.08e+03
28	Contrast	0.23 ± 0.15	0.22 ± 0.07
29	Correlation*	0.91 ± 0.02	0.93 ± 0.02
30	Energy*	0.37 ± 0.08	0.39 ± 0.06
31	Homogeneity	0.95 ± 0.02	0.95 ± 0.01
32	Entropy*	6.01 ± 0.46	6.04 ± 0.33

* Significant based on *t* test

conducted using the above configuration, and the results are presented in this section.

ALL is diagnosed on the basis of the presence or absence of unhealthy lymphocyte samples. Therefore, lymphocytes must be characterized as "unhealthy" or "healthy" cells in blood samples for the diagnosis of ALL. In the present study the total data set used for the development of the model comprises peripheral blood smear (*PBS*) samples and was collected from 54 patients diagnosed with ALL and 50 control subjects. And 150 and 120 stained subimages of lymphocyte were obtained by the image acquisition and subimaging process as described in Sect. 2 from unhealthy and healthy subjects, respectively. The subjects of the *PBS* samples were male and female between 3 and 45 years of age.

Experiments were conducted on the available lymphocyte images to demonstrate the efficacy of the image segmentation scheme and are presented in Sect. 2.5. Figures 6 and 7 show the segmented nucleus of lymphocyte and lymphoblast samples, respectively. Further, significant

differences in terms of nucleus chromatin distribution were observed between benign and malignant alterations. Such anomalies in nucleus chromatin distribution reflect the organization of the DNA and can be described in terms of texture for the classification of healthy and normal *PBS* samples.

After segmentation, nucleus and cytoplasmic features of normal and malignant lymphocytes were extracted and are summarized into mean and standard deviation and are tabulated in Tables 5, 6, 7, and 8. Further, independent-sample "*t*" test suggests that 32 features are statistically significant and have the capability enough to discriminate lymphocyte samples into malignant and benign. A plot between feature index and *p* value is depicted in Fig. 11, which indicates significance of the features to discriminate between two groups.

Table 7 Color features extracted from nucleus region of normal and malignant lymphocytes

Feature index	Features	Malignant $\mu \pm \sigma$	Normal $\mu \pm \sigma$
33	Avg. of red component*	113.84 ± 25.65	125.72 ± 20.67
34	Avg. of green component*	27.54 ± 9.31	58.66 ± 17.37
35	Avg. of blue component*	133.45 ± 27.46	138.81 ± 19.63
36	Avg. of hue component	0.80 ± 0.02	0.81 ± 0.03
37	Avg. of saturation component*	0.79 ± 0.10	0.59 ± 0.07
38	Avg. of value component*	0.53 ± 0.10	0.56 ± 0.07

Table 8 Color features extracted from cytoplasm region of normal and malignant lymphocytes

Feature index	Features	Malignant $\mu \pm \sigma$	Normal $\mu \pm \sigma$
39	Avg. of red component*	155.75 ± 31.66	166.81 ± 22.97
40	Avg. of green component*	146.95 ± 30.65	164.55 ± 19.20
41	Avg. of blue component*	174.29 ± 35.97	203.41 ± 29.62
42	Avg. of hue component	0.63 ± 0.12	0.63 ± 0.07
43	Avg. of saturation component	0.22 ± 0.08	0.23 ± 0.07
44	Avg. of value component*	0.70 ± 0.13	0.80 ± 0.11

Further, it can be observed from Tables 5, 6, 7, and 8 that most of the features are increasing steadily from normal to malignant. The nucleus/cytoplasm (N/C) ratio of the lymphoblast is twice as large as that of mature lymphocytes. The hike in this ratio is due to increased nucleus area and reduced cytoplasm and is a typical characteristic of malignant cells caused due to increased metabolic rate. Abnormal nuclear shape in lymphoblast may be because of genetic instability which can be inferred from the differences in form factor and roundness measure of cells. Difference in nucleus chromatin distribution provides important diagnostic and prognostic information and can be observed from wavelet texture measure. Due to accumulation of ribosomal and messenger RNA, the cytoplasm of lymphoblasts appears to be basophilic. Thus, the mean color intensity of cytoplasm appears to be light blue. Analysis of measured feature values shows that the lymphocyte image samples are separable and a suitable classifier with high accuracy may be used for this purpose.

In this regard, an ensemble of classifiers (EOC) has been developed for the classification of mature lymphocyte and lymphoblast in blood microscopic images. Further, to have a fair evaluation of the proposed screening system, *k*-fold

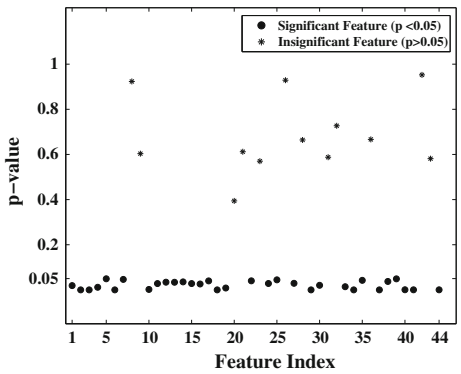

Fig. 11 Plot between feature index and *p* value for showing feature significance

Table 9 Average classification accuracy of ensemble methods along with standard classifiers over fivefold

Classifier	Fold					Avg. accuracy
	1	2	3	4	5	
NB	85.71	83.33	78.57	71.43	85.71	80.95
KNN	69.05	83.33	73.80	85.71	80.95	78.57
MLP	83.33	88.10	80.95	85.71	54.76	78.57
RBFN	80.95	90.48	76.19	66.67	80.95	79.05
SVM	92.86	95.24	95.23	85.71	88.10	91.43
EOC*	96.87	93.75	92.45	93.75	96.88	94.73

* Proposed

Table 10 Average sensitivity of ensemble methods along with standard classifiers over fivefold

Classifier	Fold					Avg. sensitivity
	1	2	3	4	5	
NB	54.54	100.00	83.33	47.06	62.50	69.49
KNN	69.23	90.91	91.67	76.92	69.23	79.59
MLP	84.62	100.00	83.33	61.54	100.00	85.90
RBFN	76.92	100.00	83.33	61.54	53.85	64.12
SVM	76.92	100.00	83.33	53.85	61.54	75.13
EOC*	96.30	95.83	94.59	92.31	95.65	94.93

* Proposed

Table 11 Average specificity of ensemble methods along with standard classifiers over fivefold

Classifier	Fold					Avg. specificity
	1	2	3	4	5	
NB	96.77	80.55	76.67	88.00	100.00	88.40
KNN	68.97	80.65	66.67	89.66	86.21	78.43
MLP	82.76	83.87	80.00	96.55	34.48	75.53
RBFN	82.76	87.10	73.33	68.97	93.10	81.05
SVM	100.00	93.54	100.00	100.00	100.00	98.70
EOC*	100.00	87.50	87.50	100.00	100.00	95.00

* Proposed

cross-validation was followed for training/testing data partitioning. Average classification performance in terms of accuracy, sensitivity, and specificity of standard classifiers such as NB, KNN, MLP, RBFN, and SVM was also evaluated along with the proposed ensemble of classifiers for 25 features, and the comparative results are presented in Tables 9, 10, and 11, respectively. It can be observed that the best overall accuracy of 94.73 is achieved with the proposed multiple-classifier system for the available *PBS* image samples with fivefold cross-validation. The corresponding sensitivity and specificity were also calculated as 94.93 and 95.00, respectively. In EOC we have observed that both accuracy and sensitivity are more than 90 % in all fivefold consistently, and the average of all folds is found to be higher than that of SVM. The corresponding specificity of EOC is also sufficiently higher than that of standard classifiers except SVM. The computational time (in seconds) that includes both training and testing phases is recorded for all the above classifiers and is presented in Fig. 12. The average computation time for EOC is found to be marginally higher than that of NB, KNN, MLP, and SVM; therefore, the proposed system can support in real clinical diagnosis.

From the above results, we conclude that EOC obtains promising results in recognizing lymphoblast from blood

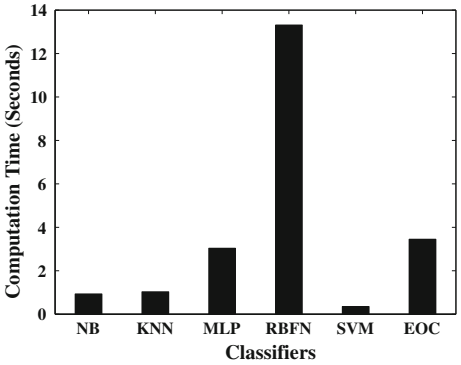

Fig. 12 Variation of computation time in seconds

microscopic images. However, we agree with the fact that much more research is necessary to completely fulfill the real clinical demand. Nevertheless, the results achieved demonstrate the potential of adopting a computer-aided approach for assisting hematologists in their final decision on suspected ALL patients.

10 Conclusion

Diagnosis of ALL in children as well as adults is one of the most important hematopathology problems. Early screening of ALL is essential and can decisively modulate the treatment plan of suspected leukemia patients. Human screening of PBS samples is always time-consuming, subjective, and inconsistent while computer-aided diagnosis of ALL from images requires specific image processing and pattern recognition tools for precise screening.

In this paper, we propose a new image processing-based tool that improves the screening accuracy of ALL in comparison with human microscopic evaluation of PBS. Initially, SCM clustering is used to segment each lymphocyte image into its individual nucleus and cytoplasm regions. During feature extraction, 44 features are extracted from segmented nucleus and cytoplasm of each lymphocyte subimages according to the malignant cell characteristics as suggested by the hematologist. Using "*t*" test, 32 statistically significant features were selected from the entire set of 44 features. These features that include both shape and texture features are used to classify the lymphocyte samples as healthy or malignant.

Using an ensemble of classifiers for the development of an automated screening system for the diagnosis of ALL from lymphocyte image samples is the main theme of the paper. Encouraging recognition accuracy was observed with the proposed multiple-classifier system in contrast to standard classifiers for *PBS* samples. Average sensitivity and average specificity of greater than 90 % are also recorded for the available images. Even though the

proposed classifier is computationally slower, the average recognition rate is much higher as required for automated acute leukemia detection. Results obtained stimulate future works that include subclassification of ALL.

References

1. Dollinger M, Ko A, Rosenbaum E (2008) Everyone's guide to cancer therapy. Andrews McMeel Publishing, Riverside
2. St. Michael's Hospital Centre for Global Health Research. University of Toronto, 2012. http://www.cghr.org
3. Castillo JJ, Mull N, Reagan JL, Nemr S, Mitri J (2012) Increased incidence of non-Hodgkin lymphoma, leukemia, and myeloma in patients with diabetes mellitus type 2: a meta-analysis of observational studies. Blood 119(21):4845–4850
4. Surveillance epidemiology and end results, 2012. http://www.cghr.org.
5. Takiar R, Nadayil D, Nandakumar A (2010) Projections of number of cancer cases in India (2010–2020) by cancer groups. Asian Pac J Cancer Prev 11(4):1045–1049
6. Arora RS, Eden TOB, Kappor G (2009) Epidemiology of childhood cancer in India. Indian J Cancer 46(4):264–273
7. Singh T (2010) Atlas and text of hematology. Avichal Publishing Company, Sirmour
8. Tkachuk CD, Hirschmann JV (2007) Wintrobe's Atlas of clinical hematology, 1st edn. Lippincott Williams and Wilkins, Philadelphia
9. Angulo J, Klossa J, Flandrin G (2006) Ontology based lymphocyte population description using mathematical morphology on colour blood images. Cell Mol Biol 52(6):2–15
10. Ghosh M, Das D, Chakraborty C, Ray AK (2010) Automated leukocyte recognition using fuzzy divergence. Micron 41(7): 840–846
11. Chakravarti GK, Bhattacharya K (2005) A handbook of clinical pathology: technique and interpretation, 5th edn. Academic Publishers, Calcutta
12. Foran DJ, Comaniciu D, Meer P, Goodell LA (2000) Computer-assisted discrimination among malignant lymphomas and leukemia using immunophenotyping, intelligent image repositories, and telemicroscopy. IEEE Trans Inf Technol Biomed 4(4): 265–273
13. Labati RD, Piuri V, Scotti F (2011) All-idb: The acute lymphoblastic leukemia image database for image processing. In: Proceedings of the 18th IEEE international conference on image processing, vol 4, pp 2045–2048
14. Kovalev VA, Grigoriev AY, Ahn Hyo-Sok (1996) Robust recognition of white blood cell images. In: Proceedings of the 13th international conference on pattern recognition 4:371–375
15. Kim KS, Kim PK, Song JJ, Park YC (2000) Analyzing blood cell image to distinguish its abnormalities (poster session). In: Proceedings of the eighth ACM international conference on multimedia, pp 395–397. ACM
16. Adollah R, Mashor MY, Mohd Nasir NF, Rosline H, Mahsin H, Adilah H (2008) Blood cell image segmentation: a review. In: Proceedings of the 4th Kuala Lumpur international conference on biomedical engineering, vol. 21, pp 141–144. Springer, Berlin
17. Liao Q, Deng Y (2002) An accurate segmentation method for white blood cell images. In: Proceedings of the IEEE international symposium on biomedical imaging, pp 245–248
18. Angulo J, Flandrin G (2003) Microscopic image analysis using mathematical morphology: application to haematological cytology. 1:304–312
19. Ko BC, Gim J, Nam J (2011) Automatic white blood cell segmentation using stepwise merging rules and gradient vector flow snake. Micron 42(7):695–705
20. Zamani F, Safabakhsh R (2006) An unsupervised gvf snake approach for white blood cell segmentation based on nucleus. In: Proceedings of the 8th international conference on signal processing, vol 2
21. Piuri V, Scotti F (2004) Morphological classification of blood leucocytes by microscope images. In: Proceedings of IEEE international conference on computational intelligence for measurement systems and applications, pp 103–108
22. Park JS, Keller JM (1997) Fuzzy patch label relaxation in bone marrow cell segmentation. In: Proceedings of the IEEE international conference on systems, man, and cybernetics 2:1133–1138
23. Sinha N, Ramakrishnan AG (2003) Automation of differential blood count. In: Proceedings of the conference on convergent technologies for Asia-Pacific region 2:547–551
24. Ongun G, Halici U, Leblebiicioglu K, Atalay V, Beksac M, Beksak S (2001) An automated differential blood count system. In: Proceedings of the 23rd annual international conference of IEEE engineering in medicine and biology society, vol 3, pp 2583–2586
25. Umpon T, Dhompongsa S (2007) Morphological granulometric features of nucleus in automatic bone marrow white blood cell classification. IEEE Trans Inf Technol Biomed 11(3):353–359
26. Ermai X, McGinnity TM, QingXiang W (2010) Automatic extraction of shape features for classification of leukocytes. In: Proceedings of the international conference on artificial intelligence and computational intelligence 2:220–224
27. Comaniciu D, Meer P (2001) Cell image segmentation for diagnostic pathology. Advanced algorithm approaches to medical image segmentation: state-of-the-art application in cardiology, neurology, mammography and pathology, pp 541–558
28. Serbouti S, Duhamel A, Harms H, Gunzer U, Aus UM, Mary JY, Beuscart R (1991) Image segmentation and classification methods to detect leukemias. In: Proceedings of the annual international conference of the IEEE engineering in medicine and biology society 13:260–261
29. Scotti F (2005) Automatic morphological analysis for acute leukemia identification in peripheral blood microscope images. In: Proceedings of IEEE international conference on computational intelligence for measurement systems and applications, pp 96–101
30. Markiewicz T, Osowski S, Marianska B, Moszczynski L (2005) Automatic recognition of the blood cells of myelogenous leukemia using svm. In: Proceedings of IEEE international joint conference on neural networks 4:2496 –2501
31. HA Hazwani, MY Mashor, R Hassan (2011) Automatic blasts counting for acute leukemia based on blood samples. Int J Res Rev Comput Sci 2(4):971–976
32. Swolin B, Simonsson P, Backman S, Lofqvist I, Bredin I, Johnsson M (2003) Differential counting of blood leukocytes using automated microscopy and a decision support system based on artificial neural networks evaluation of diffmastertm octavia. Clin Lab Haematol 25(3):139–147
33. Kratz A, Bengtsson HI, Casey JE, Keefe JM, Beatrice GH, Grzybek DY, Lewandrowski KB, Van Cott EM (2005) Performance evaluation of the cellavision dm96 system: Wbc differentials by automated digital image analysis supported by an artificial neural network. Am J Clin Pathol 124(5):770–780
34. Mohapatra S (2008) Development of impulse noise detection schemes for selective filtering. Master's thesis, National Institute of Technology Rourkela,
35. Macqueen J (1967) Some methods for classification and analysis of multivariate observations. In: Proceedings of the fifth Berkeley symposium on mathematical statistics and probability, vol 1, pp 281–297

36. Mohapatra S, Patra D (2010) Automated leukemia detection using hausdorff dimension in blood microscopic images. In: Proceedings of the international conference on emerging trends in robotics and communication technologies, pp 64 –68, December
37. Russ JC (2007) The image processing handbook, 5th edn. Taylor and Francis, Boca Raton
38. Mohapatra S, Patra D, Kumar K (2012) Fast leukocyte image segmentation using shadowed sets. Int J Comput Biol Drug Des 5(1):49–65
39. Vapnik VN (1998) Statistical learning theory. John Wiley and Sons, New York
40. Dey P (2006) Basic principles and applications of fractal geometry in pathology: a review. Anal Quant Cytol Histol 27(5):284–290
41. Busch A, Boles WW (2002) Texture classification using multiple wavelet analysis. In: Proceedings of the digital image computing techniques and applications, pp 1–5
42. Gupta L, Jayavanth S, Ramaiah A (2009) Identification of different types of lymphoblasts in acute lymphoblastic leukemia using relevance vector machines. In: Proceedings of the 31st annual international conference of the IEEE engineering in medicine and biology society, USA
43. Krishnan MMR (2010) Histopathological image analysis and machine learning methods for detection of oral submucous fibrosis. PhD thesis, Indian Institute of Technology Kharagpur
44. Samarsinghe S (2007) Neural networks for applied sciences and engineering. Auerbach
45. Krishnan MMR, Chakraborty C, Paul RR, Ray AK (2012) Hybrid segmentation, characterization and classification of basal cell nuclei from histopathological images of normal oral mucosa and oral submucous fibrosis. Expert Syst Appl 39(1):1062–1077
46. Duda R, Hart D, Stork P (2007) Pattern classification, 2nd edn. Wiley India, New York
47. Acharya T, Ray AK (2005) Image processing principles and applications. Wiley-Interscience, Hoboken
48. Haykin S (1999) Neural networks, 2nd edn. Prentice Hall, Upper Saddle River
49. Sa PK (2010) Restoration algorithms for blurred and noisy images. PhD thesis, National Institute of Technology Rourkela
50. Hansen LK, Salmon P (1990) Neural network ensembles. IEEE Trans Pattern Anal Mach Intell 12(10):993–1001
51. Polikar R (2006) Ensemble based systems in decision making. IEEE Circuits Syst Mag 6:21–45
52. Hansen LK, Salmon P (1991) Adaptive mixtures of local experts. Neural Comput 3:79–87
53. Kuncheva LI (2005) Combining pattern classifiers. Wiley-Interscience, Hoboken
54. Polikar R, Topalis A, Green D, Kounios J, Clark CM (2007) Comparative multiresolution wavelet analysis of ERP spectral bands using an ensemble of classification approach for early diagnosis of Alzheimer's disease. Comput Biol Med 37(4): 542–558
55. Zhang C, Ma Y (eds) (2012) Ensemble machine learning: methods and applications. Springer, New York
56. Krogh A, Vedelsby J (1995) Neural network ensembles, cross validation, and active learning 7:231–238